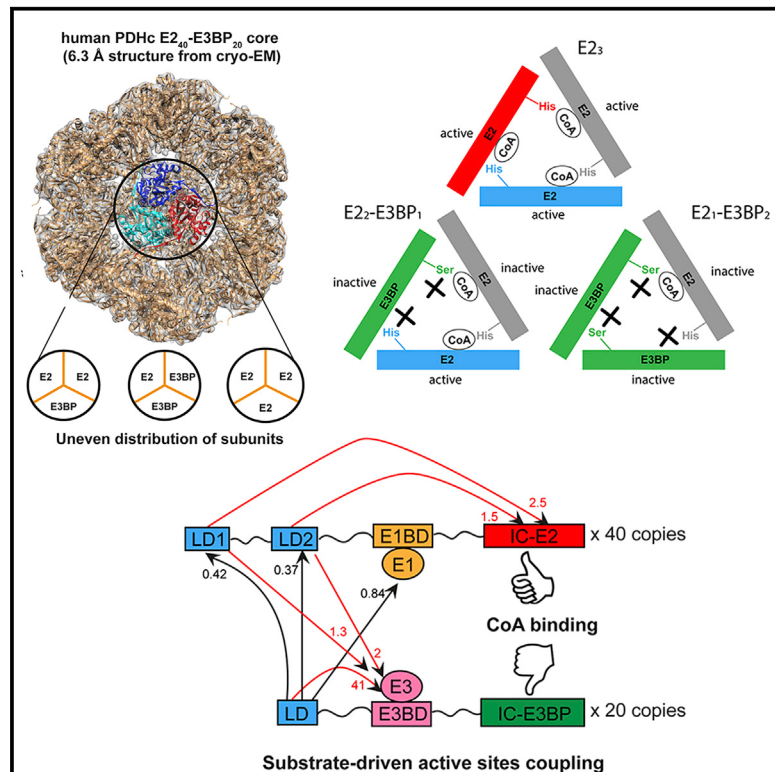


Structure

Structural and Functional Analyses of the Human PDH Complex Suggest a “Division-of-Labor” Mechanism by Local E1 and E3 Clusters

Graphical Abstract



Authors

Sabin Prajapati, David Haselbach,
Sabine Wittig, ..., Carla Schmidt,
Holger Stark, Kai Tittmann

Correspondence

cs@halomem.de (C.S.),
hstark1@gwdg.de (H.S.),
ktittma@gwdg.de (K.T.)

In Brief

Structural and functional analyses of human PDHc reveals an uneven subunit distribution in the core and periphery suggesting a “division-of-labor” mechanism of local E2-E1 and E3BP-E3 clusters during the multi-step reaction. Substrate CoA is found to modulate the conformational landscape and inter-domain coupling of PDHc extending the MRC mechanism.

Highlights

- Human PDHc E2 and E3BP subunits are structurally similar to prokaryotic PDHc E2
- E2 and E3BP are unevenly distributed in the core forming variable trimers
- Local E2-E1 and E3BP-E3 clusters catalyze different partial reactions of catalytic cycle
- Binding of CoA to E2 primes PDHc lipoyl arms for subsequent E2 and E3 reactions



Structural and Functional Analyses of the Human PDH Complex Suggest a “Division-of-Labor” Mechanism by Local E1 and E3 Clusters

Sabin Prajapati,^{1,2,6} David Haselbach,^{2,5,6} Sabine Wittig,³ Mulchand S. Patel,⁴ Ashwin Chari,² Carla Schmidt,^{3,6,*} Holger Stark,^{2,*} and Kai Tittmann^{1,2,7,*}

¹Department of Molecular Enzymology, Göttingen Centre for Molecular Biosciences and Albrecht-von-Haller Institute, Georg-August University Göttingen, Julia-Lermentowa-Weg 3, 37077 Göttingen, Germany

²Department of Structural Dynamics, Max-Planck-Institute for Biophysical Chemistry Göttingen, Am Fassberg 11, 37077 Göttingen, Germany

³Interdisciplinary Research Center HALOmem, Charles Tanford Protein Center, Institute for Biochemistry and Biotechnology, Martin Luther University Halle-Wittenberg, Kurt-Mothes-Strasse 3a, 06120 Halle/Saale, Germany

⁴Jacobs School of Medicine and Biomedical Sciences, Department of Biochemistry, University at Buffalo, 955 Main Street, Buffalo, NY 14203, USA

⁵Present address: Research Institute of Molecular Pathology (IMP), Vienna Biocenter (VBC), Campus-Vienna-Biocenter 1, 1030 Vienna, Austria

⁶These authors contributed equally

⁷Lead Contact

*Correspondence: cs@halomem.de (C.S.), hstark1@gwdg.de (H.S.), ktittma@gwdg.de (K.T.)

<https://doi.org/10.1016/j.str.2019.04.009>

SUMMARY

The pseudo-atomic structural model of human pyruvate dehydrogenase complex (PDHc) core composed of full-length E2 and E3BP components, calculated from our cryoelectron microscopy-derived density maps at 6-Å resolution, is similar to those of prokaryotic E2 structures. The spatial organization of human PDHc components as evidenced by negative-staining electron microscopy and native mass spectrometry is not homogeneous, and entails the unanticipated formation of local clusters of E1:E2 and E3BP:E3 complexes. Such uneven, clustered organization translates into specific duties for E1-E2 clusters (oxidative decarboxylation and acetyl transfer) and E3BP-E3 clusters (regeneration of reduced lipoamide) corresponding to half-reactions of the PDHc catalytic cycle. The addition of substrate coenzyme A modulates the conformational landscape of PDHc, in particular of the lipoyl domains, extending the postulated multiple random coupling mechanism. The conformational and associated chemical landscapes of PDHc are thus not determined entirely stochastically, but are restrained and channeled through an asymmetric architecture and further modulated by substrate binding.

INTRODUCTION

The pyruvate dehydrogenase complex (PDHc) is a multi-enzyme complex composed of multiple copies of three enzymes, pyruvate dehydrogenase (E1 component), dihydrolipoamide acetyltransferase (E2 component), and dihydrolipoamide dehydrogenase (E3 component). PDHc catalyzes the oxidative decarboxylation

of pyruvate, the main product of glycolysis, to acetyl-coenzyme A (CoA), which is directly fed into the tricarboxylic acid cycle, and also serves as a precursor for fatty acid and steroid biosynthesis (Korke et al., 1951; Reed, 1966). In this way, PDHc constitutes one of the key metabolic gatekeepers to control the flux of carbon from glucose to its complete combustion via cellular respiration. It is one of the largest multi-protein assemblies known, with sizes exceeding several megadaltons, and is localized in the cytoplasm of prokaryotes or in mitochondria and plastids in the case of eukaryotes (Reed, 1966; Reid et al., 1975).

In eukaryotes, the complexity of PDHc protein composition is even higher owing to the presence of additional proteins such as the E3-binding protein (E3BP), which is structurally very similar to E2 by virtue of its domain architecture (Demarcucci and Lindsay, 1985; Jilka et al., 1986; Neagle et al., 1989). However, it is supposed to be catalytically inactive due to replacement of a canonical catalytic histidine found in all E2s by a serine (Harris et al., 1997). Two regulatory enzymes, pyruvate dehydrogenase kinase (PDK, isoforms 1–4) and pyruvate dehydrogenase phosphatase (PDP, isoforms 1 and 2), regulate the activity of E1 by reversible inactivation and reactivation via phosphorylation and dephosphorylation, respectively (Kato et al., 2008; Patel and Korotchkina, 2006; Seifert et al., 2007).

In terms of structural architecture, the E2 and E3BP components assemble into a 60meric central core with icosahedral symmetry in eukaryotic PDHc (Reed and Hackert, 1990). The exact copy numbers of E2 and E3BP constituting the 60mer core is still a matter of debate. Currently, two alternative models for the E2:E3BP stoichiometry are considered as being either 48:12 (E2₄₈-E3BP₁₂) or 40:20 (E2₄₀-E3BP₂₀) (Hiromasa et al., 2004; Brautigam et al., 2009). In Gram-negative bacteria, the central core is composed of 24 E2 chains, with each of the 8 E2 trimers forming the vertices of a cubic assembly (Mattevi et al., 1992). The basic structural building blocks of all PDHc cores are either homotrimers of E2 or heterotrimers of E2-E3BP, which occupy each vertex of the corresponding cubic or icosahedral PDHc core, respectively. Adjacent trimers bind to each other via



C-terminal E2 or E3BP residues that bind to a hydrophobic pocket of the neighboring trimer. These connections resemble a ball-and-socket joint allowing high structural flexibility for spontaneous, thermally driven local contractions and retractions, thus changing the size of the core globally, in a process termed “breathing” (Zhou et al., 2001a).

In eukaryotic PDHc, the central core is decorated with E1 and E3 proteins, which bind to their respective binding domains, the E1-binding domain (E1BD) at E2 and the E3-binding domain (E3BD) at E3BP (Harris et al., 1997). In contrast, in prokaryotic PDHc the peripheral E1 and E3 components bind to the same subunit-binding domain (SBD) at E2 in a mutually exclusive manner (Mande et al., 1996; Frank et al., 2005).

One of the iconic features of PDHc catalysis is the covalent transfer of reactive intermediates between remotely located active sites at E1, E2, and E3, in a process termed covalent substrate channeling. Active-site coupling is accomplished through the action of the lipoate cofactor, which is covalently linked to a conserved lysine residue at the N-terminal lipoyl domains of E2 and E3BP, respectively (Nawa et al., 1960; Reed, 1974). These lipoyl moieties carry the acetyl group generated in the course of oxidative decarboxylation of pyruvate at E1 to the acetyltransferase site at E2. The acetyl group is transferred to bound CoA and is eventually released as acetyl-CoA. The thereby formed dihydroliopoyl cofactor is reoxidized at the active site of E3, where two reducing equivalents are transduced to a final acceptor NAD⁺. The lipoyl domains are part of a structurally extended “swinging arm,” which further contains flexible linkers between the different lipoyl domains and the SBD, as well as the lipoamide itself, which spans a distance of ~14 Å (Reed, 1974; Miles et al., 1988; Texter et al., 1988). In that way, the lipoamide cofactor is capable of visiting the active sites of E1, E2, and E3, which are spatially separated from each other by at least ~5 nm (Zhou et al., 2001b). As each E2 chain in most PDHc possesses multiple lipoyl domains (three in *Escherichia coli*, two in *Homo sapiens*), there exist more putative coupling units than active sites. Using site-directed mutagenesis as well as deletion of individual lipoyl domains, a single lipoyl domain was found to be sufficient to maintain the overall PDHc enzymatic activity, indicating a redundancy in the functioning of lipoyl domains (Guest et al., 1985; Allen et al., 1989). Also, it was predicted that the reducing equivalents or acetyl units are transferred between lipoyl domains (Bates et al., 1977; Collins and Reed, 1977; Danson et al., 1978). All of these features are consistent with a “multiple random coupling” (MRC) mechanism, in which all lipoyl domains are involved in performing the same set of reactions but each of them have the freedom to visit several active sites of the same type within the multi-enzyme assembly (Stepp et al., 1981; Hackert et al., 1983a, 1983b; Song and Jordan, 2012). Thus, at any given physiological state, the active sites would seem to be randomly coupled by lipoyl domains as a hallmark of the mechanism of PDHc and of related α -ketoacid dehydrogenase complexes.

Although PDHc and its individual enzymatic components have been studied for almost half a century, the structure and the structural dynamics of the whole complex have remained elusive so far. There are only two structures published for the central core at high resolution obtained by X-ray crystallography, both from prokaryotic PDHc, i.e., from *Azotobacter vinelandii* and

E. coli (Mattevi et al., 1992; Wang et al., 2014). In these studies, the lipoyl domains and the SBD had been removed, and the truncated PDHc core was used for structural analysis. In case of eukaryotic PDHc, most of the structural insights have been garnered from electron microscopic (EM) investigations, and the reconstructions of structural models were accomplished at moderate or low resolutions. For the human PDHc core, the highest resolutions reported so far from cryo-EM analysis amount to ~18 Å for the native E2-E3BP core, ~15 Å for the E2-only (E2₆₀) core, and ~9 Å for the truncated E2 core (tE2₆₀) devoid of the lipoyl domains and the E1BD (Yu et al., 2008; Vijayakrishnan et al., 2010). A pseudo-atomic model was calculated from the cryo-EM maps of tE2₆₀ describing the structure of human E2 core-forming inner catalytic (IC) domain. However, a recent molecular dynamics (MD) simulation-based study has predicted this structural model to be thermodynamically unstable and probably not fully accurate (Hezaveh et al., 2016).

Due to the lack of an atomic or pseudo-atomic structure of a fully assembled PDHc, the exact distribution of its components in the core and the outer shell remain unknown. Importantly, a potential variation in the distribution of E2 and E3BP in the core would result in a likewise variation in the positions of their cognate binding partners E1 and E3. Also, although it is well accepted that E1 indeed forms an outer shell around the inner core of the eukaryotic PDHc (Wagenknecht et al., 1991; Zhou et al., 2001b), the E3 component has been proposed to be either docked into the pentagonal openings (5-fold symmetry axis of the core), or, alternatively, to lie along the E1 shell (Stoops et al., 1997; Zhou et al., 2001b; Hiromasa et al., 2004). The subunit distribution might play an important role in not only the enzymatic activity but also in the regulation by PDK and PDP, which bind to E2 lipoyl domains (Rahmatullah et al., 1989).

Here, we present the pseudo-atomic structural model of the physiological E2-E3BP core of the human PDHc. We quantitatively analyzed the stoichiometry between the various components and their relative distribution for *in vitro* reconstituted human PDHc. We observed a non-homogeneous distribution of the different components in human PDHc suggesting a “division-of-labor” mechanism for locally formed, distinct (E2-E1) and (E3BP-E3) clusters. Furthermore, our studies indicate that binding of the substrate CoA to the human PDHc core affects the conformational landscape and coupling of the core and the whole PDHc. These observations necessitate revisiting the proposed MRC mechanism and instigating similar investigations regarding the role of the other PDHc substrates, pyruvate and NAD⁺, for conformational sampling and substrate channeling in future studies.

RESULTS

3D Pseudo-atomic Model of Human PDHc E2-E3BP Core

We determined the structure of recombinantly expressed E2-E3BP core of human PDHc by single-particle cryo-EM at a resolution of 6.3 Å, imposing icosahedral symmetry (Figures 1A and 1B). This core consists of full-length E2 and E3BP subunits, and its reconstitution with recombinantly expressed human E1 and E3 components yields an enzymatically fully active PDHc. The final 3D map of the core, however, only includes densities from the rigid, structurally well-defined IC domains, whereas

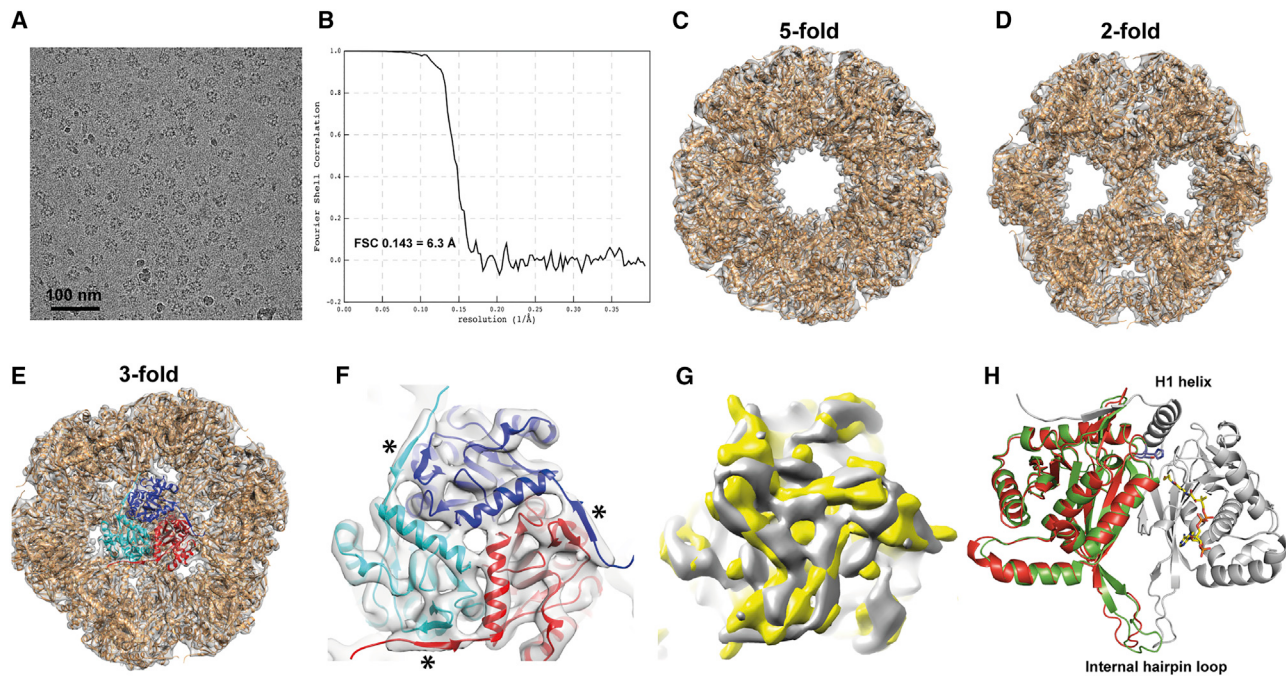


Figure 1. Cryo-EM Structure of the Human PDHc Full-Length E2₄₀-E3BP₂₀ Mixed Core in the Presence of Substrate CoA

(A) Representative cryo-EM micrograph of a recombinantly expressed human PDHc E2-E3BP core. The protein samples were pre-incubated with 2 mM CoA prior to GraFix fixation.

(B) Fourier shell correlation (FSC) curve of the cryo-EM 3D reconstruction map for the E2-E3BP core estimated the resolution as 6.3 Å.

(C-E) Structural model of the 60mer core consisting of 60 inner catalytic domains of E2 (IC-E2₆₀) fitted into the EM map as a pentagonal dodecahedron displayed at its 5-fold (C), 2-fold (D), and 3-fold (E) symmetry axes.

(F) A trimer of the core is highlighted with the three E2 monomers colored individually in red, cyan, and blue. Asterisks indicate short β strands at the N terminus of the core-forming IC domains, which form an anti-parallel β sheet with an internal β strand of a neighboring subunit in the trimeric unit.

(G) Comparison between the EM reconstruction map of the E2-E3BP core at 6.3 Å resolution (gray) with that of the tE2 core (yellow) (Yu et al., 2008). The trimer is viewed down the 3-fold symmetry axis.

(H) An alignment of pseudo-atomic models of IC-E2 (red) and IC-E3BP (green) monomers indicates similar 3D structures of the two components. Helix H1 and an internal hairpin loop represent the outermost and innermost part of the core relative to the center of mass. A CoA molecule binds to a neighboring E2 subunit (gray) through a long substrate channel from inside the core with its thiol pointing toward a catalytic histidine (blue, underneath helix 1) contributed from neighboring E2 (red) of the same trimer. At the equivalent position in E3BP (green), the histidine is replaced by a catalytically inactive serine (coordinates for the CoA molecule were derived from PDB: 1EAD).

the N-terminal lipoyl domains, SBDs (E1BD, E3BD), and the corresponding inter-domain linkers are filtered out due to their high conformational flexibility (Figures 1C–1E, Video S1). Likewise, no density could be traced for the substrate CoA, which had been added at saturating concentrations to the sample. For some of the flexible linkers, though, density is observed emanating from the core in the 2D class averages (Figure S2). Consistent with earlier observations made in the case of the previously reported tE2 structure (Yu et al., 2008), small portions of these linkers are also visible in the 3D map at a lower density threshold (Figure S2).

The two independently calculated pseudo-atomic models of the IC domains of E2 (IC-E2₆₀) and E3BP (IC-E3BP₆₀) derived from the cryo-EM map of the E2-E3BP mixed core particles are almost identical (Figure 1H). This was an expected outcome, as both proteins share nearly 50% sequence similarity in their core-forming IC domains and are thus likely to adopt a very similar fold (Harris et al., 1997).

The visually defining structural elements of a trimeric unit, which form the vertices of the pentagonal dodecahedron, are

the surficial H1 helices. They are organized into a characteristic tripetal flower-like arrangement (Figures 1F and 1G, Video S1). The spatial orientation of the H1 helix has been proposed to be different between prokaryotic and human PDHc E2, with the human version being rotated ~20° away from the 5-fold symmetry axis (Yu et al., 2008). In the structure of the physiological human PDHc core presented herein, however, we do not detect such rotation of H1. The orientation of the H1 helices in our structural models is highly similar to those reported for prokaryotic PDHc E2 upon structural alignment (Figure 2). Despite good overall agreement of our newly determined structure with the previously reported tE2 core structure, several structural differences between the models could be identified including (1) the orientation of helix H1, (2) two small antiparallel β strands between helix H3 and strand S2 previously modeled as a loop for tE2, (3) an internal loop region where we observe another small β strand in our model, and (4) an internal hairpin loop with two connected antiparallel strands (Figures 2 and S1). At present, we cannot distinguish whether the observed structural differences are a consequence of different biochemical composition (physiological

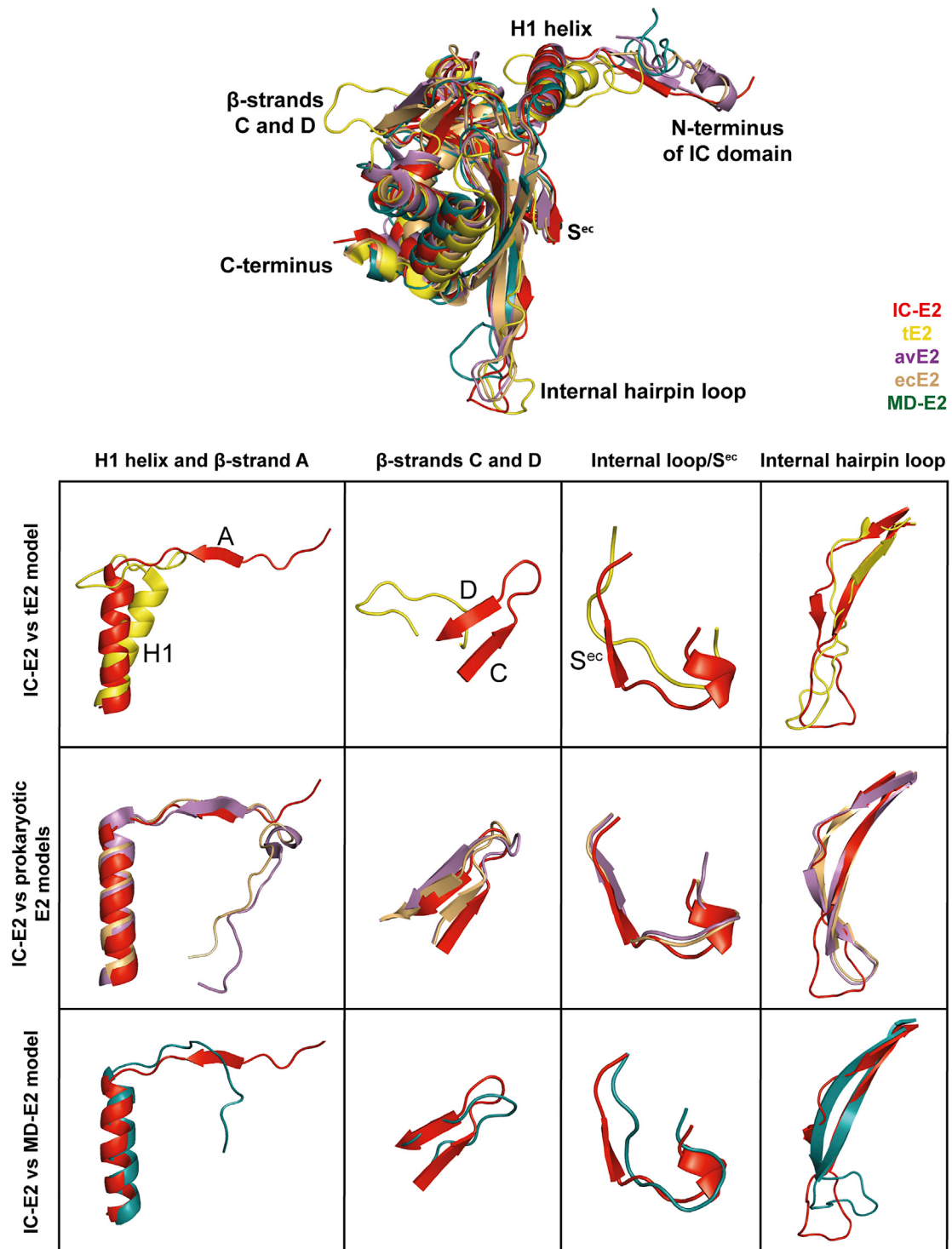


Figure 2. Alignment of the Newly Determined E2 Model with Prokaryotic PDHc E2, Human tE2, and MD-E2 Models

Alignment of the newly determined E2 model (IC-E2 in red) with those from *A. vinelandii* (avE2 in purple, PDB: 1EAD), *E. coli* (ecE2 in green, PDB: 4N72), human tE2 (yellow, PDB: 3B8K) and E2 model derived from MD simulation (MD-E2 in green, [Hezaveh et al., 2016](#)). Interestingly, IC-E2 shows a higher resemblance to those from bacterial sources and MD-E2 rather than the previously determined structure of human E2 (tE2). The structural regions, where major differences between IC-E2 with tE2 are detectable are highlighted separately, as well as the corresponding comparison with other E2 structures. The nomenclature of the structural regions is detailed in [Figure S1](#).

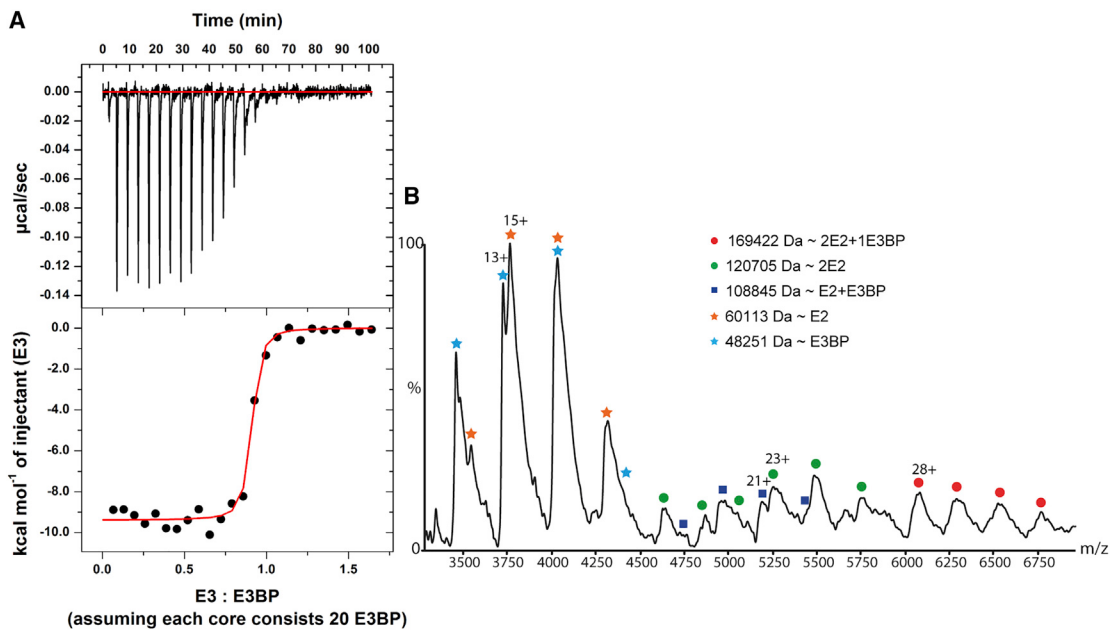


Figure 3. Subunit Stoichiometry and Distribution in Human PDHc

(A) Microcalorimetric analysis of the interaction of the E2-E3BP core with E3. In a typical ITC experiment, 140–210 μM E3 dimer was titrated to 0.5–1.5 μM human PDHc core at 25°C. The heat of binding for each titrant injection (inverted peaks, upper panel) was integrated, and the heat of dilution from the control experiment was subtracted to obtain a binding isotherm (bottom panel), which was plotted according to one-set-of-sites model fitting in the MicroCal Analysis software. The concentration of E3BP was calculated considering either the E2₄₀-E3BP₂₀ or the E2₄₈-E3BP₁₂ model. A data fit is shown in the lower panel (red line) assuming the E2₄₀-E3BP₂₀ model results in a stoichiometry of one E3 dimer per E3BP chain ($N = 1.04$, SEM = 0.05). When one assumes the E2₄₈-E3BP₁₂ model, almost two E3 dimers would bind to one E3BP chain ($N = 1.89$, SEM = 0.05), which is impossible. The data provided here are averages from five independent experiments carried out with three independent batches of protein purifications.

(B) Native mass spectrometric analysis of human PDHc E2-E3BP core, in which building blocks could be identified. Peaks for monomeric E2 and E3BP, E2₂ homodimer, E2-E3BP heterodimer, and E2₂-E3BP₁ heterotrimer could be resolved. The broad peaks likely represent the heterogeneity in lipoylation states of the lipoyl domains of E2 and E3BP.

E2-E3P core versus tE2 core) and/or differences in the preparation of cryo-EM grids. Nevertheless, it is noteworthy that the structure of the physiological E2-E3BP core reported here displays a high resemblance with the core structures of *A. vineelandii* and *E. coli* both determined by X-ray crystallography, and the structure of human E2 obtained by *in silico* modeling (MD-E2 (Hezaveh et al., 2016)) (Figure 2).

Binding of Peripheral Proteins in Human PDHc Core

We were able to improve the resolution of the human PDHc E2-E3BP core structure to ~ 6 Å. However, from examples of icosahedral viruses, it is well established that one could easily achieve resolutions of ~ 3 Å with the number of particles we employed here. We therefore wondered whether conformational heterogeneity was limiting in order to achieve higher resolution. At the ~ 6 -Å resolution attained here, E2 and E3BP chains still remain undistinguishable. Consequently, the exact number of E2 and E3BP chains in a PDHc 60mer core cannot be quantitatively assessed by relying solely on this structural information. To tackle this question, we used isothermal titration microcalorimetry (ITC), and analyzed the thermodynamics of the biophysical interaction of the E2-E3BP core with E1 as well as with E3. The estimated stoichiometries of E1:(E2-E3BP) and (E2-E3BP):E3 should indicate the ratio between E2 and E3BP in the 60mer core. The ITC analysis revealed that ~ 20 E3 dimers bind to a sin-

gle human E2-E3BP PDHc core as used for our structural analysis (Figure 3A). Unfortunately, in the case of E1, protein aggregation during the ITC experiment prevented a reliable quantitative analysis. Our results regarding the binding of E3 mirror previous results reported by Brautigam et al. (2009). This finding also sheds new light onto two controversially discussed features of the human PDHc structure: first, the relative abundance of E3BP in the core (E2₄₀-E3BP₂₀ versus E2₄₈-E3BP₁₂ models) and second, the stoichiometry of E3 binding to an individual E3BP subunit (1 E3 dimer: 1 E3BP versus 1 E3 dimer: 2 E3BP). As the stoichiometry between the E3 dimer and E3BP was found to be 1 (assuming each core to consist of 20 E3BP chains), it can be concluded that—at least in our hands and when studying recombinantly expressed proteins—human PDHc core would be best described with a E2₄₀:E3BP₂₀ model with each E3BP chain binding one E3 dimer, much like as suggested by the crystal structure analysis of the E3-E3BD subcomplex (Ciszak et al., 2006).

We further analyzed the human PDHc core by native mass spectrometry (Figure 3B). The mass spectrum shows several species between 3,000 and 7,000 m/z. The masses of two species (orange and cyan stars) correspond to E2 and E3BP monomers. Broad peaks of both subunits indicate different degrees of lipoylation of the lipoyl domains (two domains for E2, one domain for E3BP). We further identified two higher mass species corresponding to

the E2 homodimer and the E2₂-E3BP₁ heterotrimer. We also identified an E2-E3BP heterodimer, albeit at lower intensities.

Distribution of the Peripheral Proteins and Core Components in the Human PDHc

Next, we analyzed the spatial distribution of the peripheral E1 and E3 components on the core. We anticipated a homogeneous distribution of the E1 and E3 components at the outer shell decorating the inner E2-E3BP core. Considering an E2₄₀-E3BP₂₀ model with an even distribution of E2 and E3BP, this would translate into 20 E2₂-E3BP₁ heterotrimers constituting the dodecahedral icosahedron. To test this hypothesis, we performed negative-stain EM analysis of *in vitro* reconstituted (1) human PDHc (fully assembled), (2) E1:(E2-E3BP) subcomplex, and (3) (E2-E3BP):E3 subcomplex, respectively. In the raw EM micrographs, the fully reconstituted PDHc and the E1:(E2-E3BP) subcomplex exhibited similar sizes with a diameter of ~45 nm (Figure S3). For both samples, only few particles seem to be symmetrically decorated by the outer shell components. The E1 and E3 components cannot be structurally discerned in the case of the full complex, and thus their individual distributions cannot be reliably analyzed. However, in the case of the (E2-E3BP):E3 subcomplex, distinct E3 clusters are clearly detectable (Figure 4A). Addition of the PDHc substrates CoA (binds to E2) or NAD⁺ (binds to E3) did not change this inhomogeneous distribution (data not shown). This observation implies a heterogeneous distribution of the E2 and E3BP chains in the E2₄₀-E3BP₂₀ core of assembled PDHc. If the E2₄₀-E3BP₂₀ core was to be predominantly formed by (E2₂-E3BP₁)-type trimers, E3 should not form large clusters or patches at the surface of the core but rather be evenly distributed on the core. To gather additional insights into the structural organization of the building blocks making up the core, we carried out native mass spectrometry analyses of fully assembled human PDHc. This revealed the unanticipated existence of (E2₁-E3BP₂)-type heterotrimers for the very first time (Figure 4C). A related important observation we made during native mass spectrometry analysis was the detection of higher oligomers, namely dimers and trimers of the (E2₁-E3BP₂) heterotrimers, strongly suggesting the existence of local E3BP clusters in the core and, consequently, E3 and E1 clusters at the periphery of the PDHc assembly. The spectra attributable to ~263-kDa species unambiguously proves the existence of such a trimer as it can only arise from the E3:(E2₁-E3BP₂) subcomplex. Interestingly, when we analyzed isolated human PDHc E2-E3BP core (no reconstitution with E1 and E3), only the “expected” (E2₂-E3BP₁)-type trimer was observed in addition to E2 homodimers and E2-E3BP heterodimers (vide supra), suggesting that binding of the peripheral components induces spatial clustering of the core components and the peripheral components.

To exclude the possibility that E1 and E3 form larger oligomers on their own, we also performed control experiments with highly concentrated E1 and E3 components (Figure S4). Here, we observed only species with *m/z* ratio fitting to their corresponding quaternary structures (E1: $\alpha_2\beta_2$ heterotetramer; E3: α_2 homodimer). Intriguingly, we observed several species corresponding to higher oligomer of the E2₁-E3BP₂ trimer in the case of E1:(E2-E3BP) subcomplex, much like as observed for fully assembled PDHc, corroborating our hypothesis of local clusters of the various components both in the inner core and the periphery.

CoA-Binding Capacity of E2 and E3BP

Although compelling evidence exists that E3BP has lost its catalytic ability for the acetyltransferase reaction due to a His→Ser mutation of a conserved catalytic histidine found in all hitherto known E2, its ability for binding of substrate CoA has remained uncharacterized. The function of E3BP could, at least in theory, be more than just an anchor for E3 and the provision of an additional lipoyl domain for acyl and redox transfer and active-site coupling. We considered the possibility that E3BP might also act as a sink for CoA molecules for ready supply to nearby E2 chains, or alternatively for acetyl-CoA formation facilitated by the canonical histidine provided by a neighboring E2 chain in an E2-E3BP heterotrimer.

We thus carried out ITC experiments to quantitatively assess the stoichiometry of CoA molecules binding to the E2₄₀-E3BP₂₀ core (Figure 5A). When assuming that all 60 chains of the core would bind CoA, the stoichiometry between CoA per chain of the 60mer core was determined to be *n* = 0.66. When one assumes that only E2 chains are capable of binding CoA, the stoichiometry between binding site and CoA was found to be ~1. As a control, we carried out the same ITC experiments with the artificial E2₆₀ core (devoid of E3BP), which yielded a binding stoichiometry of 0.92 ± 0.05 between E2 monomer and CoA (Figure S5). This showcases that E3BP has not only lost its enzymatic acetyltransferase activity but moreover does not bind CoA. As mentioned before (vide supra), human PDHc core is very likely a mixture of several types of trimers with varying composition of E2 and E3BP chains. The enzymatic acetyltransferase activity of such trimers is reduced when E3BP is present (Figure 5B). For E2₃-type trimers, each of its three chains binds CoA and donates a catalytic histidine to its immediate neighbor in the trimeric assembly comprising three functional active sites. When one E3BP replaces an E2 chain in (E2₂-E3BP₁) heterotrimer, only one E2-harbored active site receives the catalytic histidine from the second E2 chain of the E2₂-E3BP₁ trimer and thus retains catalytic activity, drastically reducing the number of catalytically active sites to one per trimer. This is an immediate consequence of E3BP neither binding CoA nor providing the catalytic histidine to a neighboring E2 chain. Likewise, a heterotrimer consisting of two E3BP and one E2 chain (E2₁-E3BP₂), or consisting of only E3BP, completely loses acetyltransferase activity (Figure 5B).

Interactions of the E2 and E3BP Lipoyl Domains Identified by Crosslinking Mass Spectrometry

The structural architecture of the PDHc entails that the lipoyl domains of both E2 and E3BP are functionally redundant, and are all capable of catalyzing acyl and redox transfer between the active sites at E1, E2, and E3. We employed crosslinking mass spectrometry to map the physical interactions of *in vitro* reconstituted human PDHc. Our analyses revealed that the two lipoyl domains of E2 form crosslinks with several lysine residues at the surface of E1 and E3 at the periphery as well as with lysines at the IC domains of E2 and E3BP, indicating a high conformational flexibility of these domains and the associated inter-domain linkers (Table S3). In contrast, the lipoyl domain of E3BP formed only few crosslinks with E1 but numerous crosslinks with E3. It further makes contact with the lipoyl domain 2 of E2 and the IC domain of E3BP. When only lysine residues

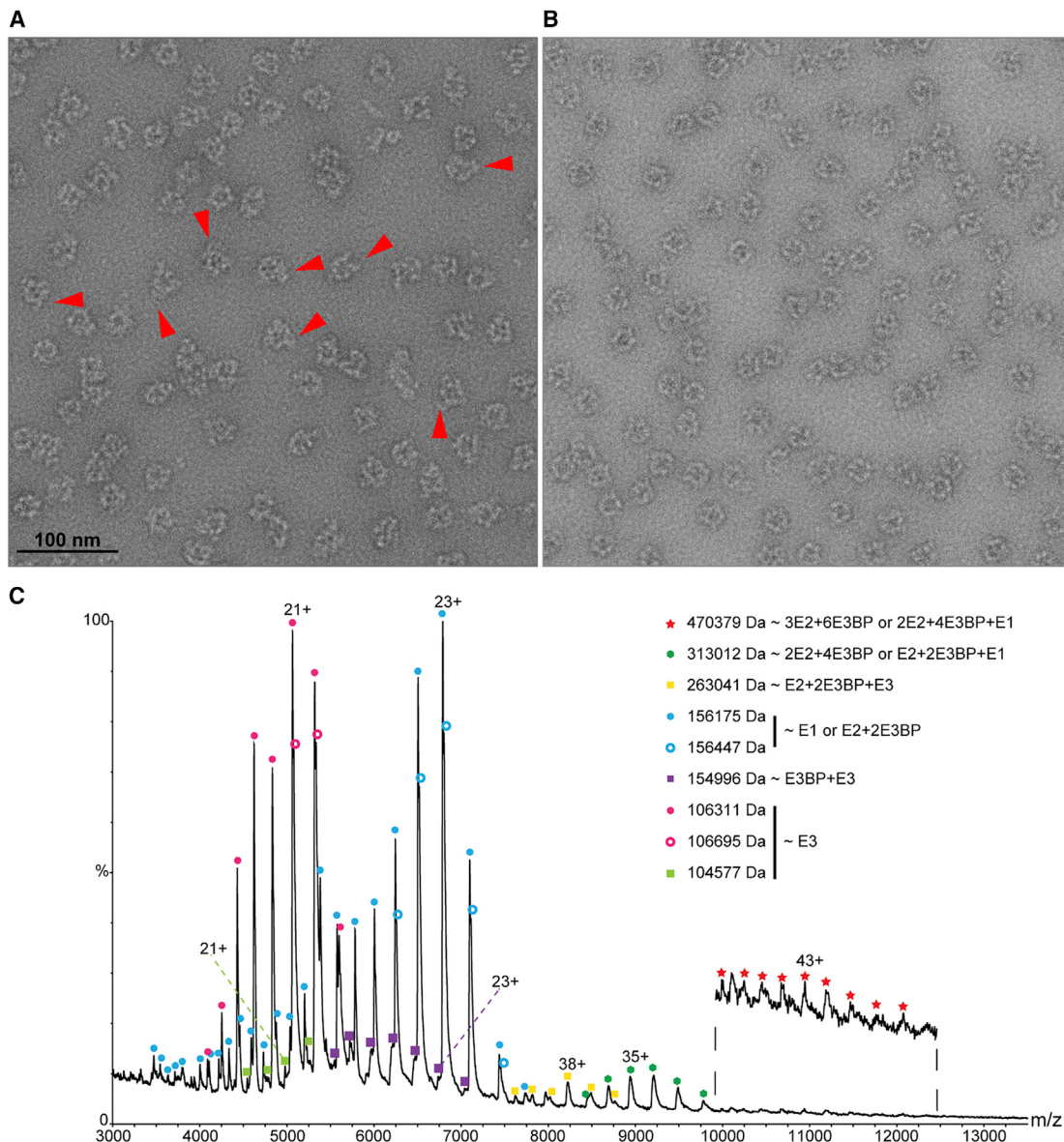


Figure 4. Negative-Staining EM and Native Mass Spectrometry Studies on Human PDHc and Subcomplexes

(A) Negative-staining EM micrograph of (E2-E3BP):E3 subcomplex reveals extra densities near the surface of the core (red arrowheads), likely originating from bound E3 molecules.

(B) These structural features were not observed for the isolated E2-E3BP core. The distribution of such densities was not homogeneous, suggesting the formation of different types of trimers within a single core, including E2₃, E3BP₃, E2₂-E3BP₁, and E2₁E3BP₂. The image was recorded at a pixel size of 2.5 Å/pixel.

(C) The human PDH complex in fully assembled form also fragmented during native mass spectrometry analysis akin to the analysis of the isolated core, however, building blocks larger than trimers were also detected. The detected species represent clusters of a previously undetected trimer arrangement between E2 and E3BP, i.e., E2₁-E3BP₂ heterotrimer and higher oligomers thereof.

close to the lipoyl entrance site of E1, E2, and E3 are considered to be relevant, the same pattern is observed (Figures 6C–6E). This finding implies a functional specificity of the E2 and E3BP lipoyl domains in PDHc catalysis, although they are chemically and structurally highly similar.

Next, we analyzed the impact of substrate binding on the structure and structural dynamics of human PDHc. To this end, we quantified the abundance of selected crosslinks, in which lysine residues are close to lipoyl entrance sites of all the compo-

nents (E1, E2, E3), in the presence and absence of substrate CoA, which binds to E2 of the PDHc without further enzymatic processing (Table S2). Earlier studies suggested that binding of CoA might prime the PDHc for acyl transfer reaction at the active site of E2 (Kato et al., 2006). In the presence of CoA, the lipoyl domains of E2 and E3BP did not show an overall change in crosslinking abundance with lysine residues close to the E1 lipoyl entrance site. However, the abundance of crosslinks between the lipoyl domains of E2 and lysine residues close to E2

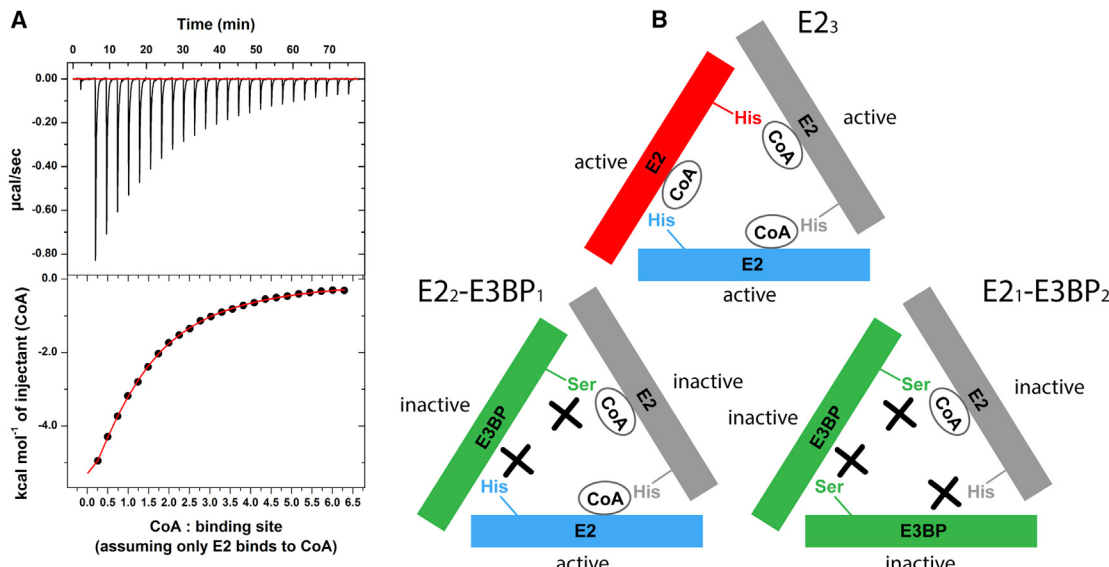


Figure 5. Coenzyme A-Binding Capacity of the Human PDHc E2-E3BP Core and Implications for the Acetyl Transferase Activity of Core Homo- and Heterotrimers

(A) Microcalorimetric analysis of CoA binding to E2-E3BP mixed core of human PDHc. A 1:1 stoichiometry (0.989, SEM = 0.08) between CoA and E2 was calculated, when 40 E2 subunits were assumed to bind CoA in a PDH core. When the 20 E3BP subunits were also assumed to bind CoA in addition to the 40 E2 chains, the stoichiometry between CoA and the core-binding sites was determined to be 0.66 (SEM = 0.05). Three independent experiments were carried out using 2 mM CoA and 1.5 μM human PDHc core.

(B) Acetyl transferase activity of different human core trimers taking into account the ability to bind CoA (E2 yes, E3BP no) and to donate a catalytic histidine to a neighboring active site (E2 yes, E3BP no). In an E₂₃ homotrimer, all three active sites are catalytically active and capable of binding CoA. When one E2 chain is replaced by E3BP to form an E₂-E₃BP₁ heterotrimer, only one of the potential three active sites exhibits acetyl transferase activity. In the case of an E₂₁-E₃BP₂ heterotrimer, all the active sites are catalytically non-functional.

lipoyl entrance sites of E2-IC increased almost 2.5-fold. Even more intriguing, the crosslinks between the lipoyl domain of E3BP and E3 increased 41-fold, and 2-fold in the case of the lipoyl domains of E2. This observation indicates that CoA binding to the core primes the lipoyl arms to move toward the interior of the core, the E2 active site, as well as toward the E3 protein in the periphery, which seems logical because the role of CoA in the PDHc reaction starts after the E1 reaction. Additionally, the number of crosslinks between the lipoyl domain of E3BP and the two lipoyl domains of E2 decreased by more than 2-fold, which implies a marked change in the inter-lipoyl redox exchange reaction as the lipoyl domains are now much inclined toward the E2 and E3 active sites.

DISCUSSION

Structural Organization of Human PDHc

Pseudo-atomic structural models of the native human E2-E3BP PDHc core were determined at a resolution of ~6 Å. The N-terminal lipoyl domains and SBDs are nonetheless invisible due to their innate structural plasticity and that of the connecting linkers. Since PDHc cores are known to be soft and structurally dynamic (Kong et al., 2003), we had added the substrate CoA and further employed chemical crosslinking (GraFix method (Kastner et al., 2008)) to potentially rigidify PDHc in the quest for increased resolution.

Our calculated E₂₆₀ and E3BP₆₀ structural models of the central 60mer core are very similar to the published crystal struc-

tures of E2 IC domains of prokaryotic PDHc but different to the cryo-EM structure of N-terminally truncated human E2 devoid of the lipoyl and SBDs (tE2). The previously published tE2 structure was calculated from the ~9-Å cryo-EM map of a non-native E2-only (E₂₆₀) core, which was suggested to be structurally different compared with the *A. vinelandii* E2 crystal structure at different loci such as an internal hairpin loop and the helix H1 orientation. Our structural analysis could not confirm the structural differences with respect to prokaryotic PDHc E2. Our observations are rather in accord with recently published human E2 and E3BP structures obtained by homology modeling and MD simulations, which also suggested that the published tE2 structure may not be fully accurate (Hezaveh et al., 2016). As these differences were perceived to be key determinants responsible for the different overall organization of the core between eukaryotic (E2-E3BP mixed core) and prokaryotic (E2-only core) PDHc cores, our data suggest that such organizational variation is unlikely due to structural differences, at least not at the monomeric level of E2 and E3BP.

Our biophysical interrogation further revealed that the human PDHc core binds 20 E3 α₂ dimers at full saturation supporting the E₂₄₀E₃BP₂₀ model, and at the same time rendering the E₂₄₈-E3BP₁₂ model to minor probability. Also, the previous proposition that two E3BP chains simultaneously bind one E3 dimer in solution (Smolle et al., 2006) as opposed to the 1:1 binding observed *in crystallo* (Ciszak et al., 2006) must be refuted. As (E₂₁-E3BP₂)-type heterotrimers were detected as major building blocks of human PDHc during native mass spectrometric

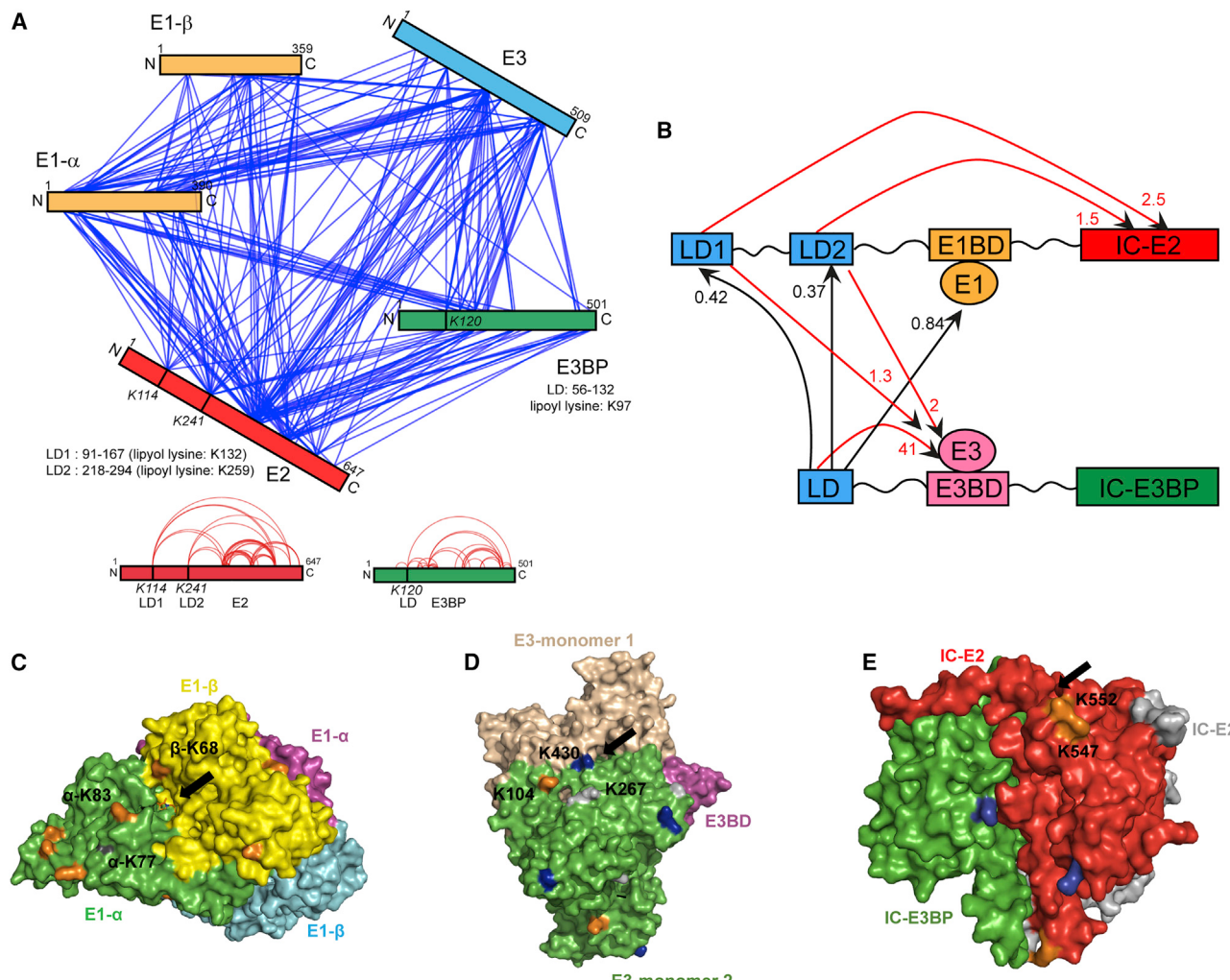


Figure 6. Mass Spectrometric Analyses of Crosslinks Formed within Human PDHc

(A) A map of detected crosslinks between all components of human PDHc is shown (inter-subunit crosslinks in blue and intra-subunit crosslinks in red). (B) Schematic representation of the quantitative changes of crosslinks of the E2 and E3BP lipoyl domains upon addition of substrate CoA relative to the resting state enzyme. An increased movement of E2 lipoyl domains toward the E2 core (1.5- to 2.5-fold increase) and toward E3 (2-fold increase), a decreased crossstalk between the E2 and E3BP lipoyl domains (>2-fold decrease), and a dramatically increased movement of the E3BP lipoyl domain toward E3 (40-fold increase) were observed upon addition of CoA. In addition, a slightly decreased amount of crosslinks between the E3BP lipoyl domain and E1 (0.8-fold) was detected. The frequency of crosslinks between LD2 with α -83 and β -68 residues of E1 changed in an equivalent but opposite manner, so no conclusion could be made regarding E2-LD movement to E1 upon CoA addition. A complete list of crosslinkings used for quantification is detailed in Table S2.

(C-E) Structures of the E1 $\alpha_2\beta_2$ heterotetramer (C, PDB: 1NI4), E3 α_2 homodimer (D, PDB: 1ZY8) and E2-E3BP₁ heterotrimer (E) with the lipoyl entrance sites highlighted by black arrows. The crosslinks that were exclusively observed for E2 lipoyl domains are highlighted in orange, those exclusive for E3BP are shown in blue and common crosslinks are shown in gray. For the sake of clarity, only crosslinking lysine residues close to lipoyl entrance sites are indicated.

analysis (Figure 4C), an uneven distribution of the E3BP chains within the core must be deduced. In consequence, this also implies an uneven distribution of E1 and E3 components at the periphery of PDHc, as evident for example in the EM micrographs of the (E2-E3BP):E3 subcomplex.

In contrast, we observed the expected (E2-E3BP₁)-type trimer for isolated human PDHc core but not the (E2₁-E3BP₂)-type heterotrimer as detected for the fully assembled complex (Figure 3B). From a functional perspective, since E3BP neither binds CoA nor lends a catalytic histidine to a neighboring chain in the trimer (Figure 5B), it is catalytically beneficial for the human

PDHc to consist of a core with mainly E2₃ homotrimers and (E2₁-E3BP₂) heterotrimers as separated clusters. This structural arrangement is capable of yielding up to 30 active acetyltransferase sites (10 E2₃ trimers + 10 E2₁-E3BP₂ trimers). In contrast, only 20 active sites would be available in comparison if the whole core was made up of 20 E2₂-E3BP₁ heterotrimers and assuming an even distribution of all components.

The experimental observation of the (E2₁-E3BP₂)-type trimer and higher oligomers thereof will also serve as an additional parameter for future modeling studies of subunit composition in eukaryotic PDHc. In a previous study, a constraint allowing

only one E3BP per trimer unit was applied, most likely due to the absence of evidence for higher oligomers of E3BP alone (Vijayakrishnan et al., 2011). The observation of two E3BP subunits in a trimeric building unit further highlights that the variation and complexity in the spatial organization of the core is higher than anticipated, especially since the exact number of such trimers in a single PDHc core still remains unknown. Additionally the ability of E3BP to form inter-trimer linkages with E2 and/or E3BP from a neighboring trimer unit needs further exploration for defining the determinants for correct assembly of the core.

Another functional advantage of local E2:E1 and E3BP:E3 clusters concerns the regulation of the activity of E1 by PDKs, which are thought to hop between lipoyl domains of neighboring E2 chains. Since PDKs bind stoichiometrically to PDHc with only 1–2 copy numbers per PDHc molecule (Liu et al., 1995), they will operate more efficiently when many E2:E1 units are locally clustered rather than homogeneously distributed.

Division-of-Labor Mechanism

A direct consequence of local E2₃ and E2₁-E3BP₂ clusters of the human PDHc core would be separated working locales for the E1 and E3 enzymes at the periphery. In the course of the PDHc reaction cycle, the lipoyl domains of E2 and E3BP need to visit the active sites at E1, E2, and E3 in a successive manner. Thus, it seems at first sight disadvantageous if E1 and E3 would be kept separated in clusters and not evenly distributed. On the other hand, inter-lipoyl-domain coupling might help in shuttling the reducing equivalents from E1-rich sites to E3-rich sites for eventual reoxidation of the dihydrolipoamide cofactor. According to such a mechanism, a single lipoyl domain would not need to visit all the active sites at E1, E2, and E3 but would rather have preferred functional roles at different stages of the PDHc multi-step reaction. Pyruvate decarboxylation, reductive acetylation of lipoamide, and CoA *trans*-acetylation would occur at E1-E2 clusters, whereas dihydrolipoamide reoxidation would preferentially take place at E3BP-E3-rich sites. The detected inability of E3BP to bind substrate CoA, thereby rendering a E2₁-E3BP₂ type trimer completely catalytically inactive (acetyltransferase activity, see Figure 5), also supports this “division-of-labor” mechanism.

Another major consequence of such organization of human PDHc is that the lipoyl domain of E3BP will be inefficient in reaching the active site at E1 as supported by our crosslinking mass spectrometry studies (Figure 6A). On the contrary, the lipoyl domains of E2 are capable of reaching all the active sites of PDHc. This observation reaffirms and rationalizes the previously reported functional non-equivalence between the lipoyl domains of E2 and E3BP despite the fact that they are chemically and structurally almost identical. In those studies, lipoyl arms of E2 or E3BP of a eukaryotic PDHc were cleaved off using proteases such as collagenase and Arg-C. Thus, obtained PDHc samples retained ~80% of the overall activity when the E3BP lipoyl domain had been removed, whereas only 10% residual activity was detected for those PDHc lacking the E2 lipoyl domains (Rahmatullah et al., 1990; Neagle and Lindsay, 1991). The spatial restrictions of the E3BP lipoyl domain to access the E1 surface and active site results in decreased participation in E1 reaction, which is another contributing factor underpinning the division-of-labor mechanism.

Similar division in catalytic duties, albeit between E2 chains, might also exist in prokaryotic PDHc. One of the proposed models for *E. coli* PDHc includes such a phenomenon in a functional E2 homotrimer (Song and Jordan, 2012). While the first E2 chain would be exclusively dedicated to catalyze the E1 reaction, its reductively acetylated lipoyl group would then visit the acetyltransferase active site of one of its neighboring E2 chains. Finally, the reducing equivalents are transferred from its lipoyl group either directly to E3 bound to the third E2 neighbor of the trimer unit, or alternatively to its lipoyl domains. Our established cross-linking mass spectrometry is unfortunately not applicable, since lipoyl domains from one E2 chain cannot be differentiated from another E2 chain as opposed to E3BP and E2 in the case of human PDHc.

However, such a mechanism in part contrasts with and also extends the classic MRC mechanism of PDHc action that would predict unrestricted conformational flexibility for all lipoyl arms such that lipoyl domains from multiple chains can visit each of the various active sites of E1, E2, and E3. The mechanism entails a stochastic conformational sampling of all lipoyl domains independent of each other but connected by inter-lipoyl-domain transfer of acetyl group and reducing equivalents (Reed and Hackert, 1990). Although our observations agree with hallmarks of MRC mechanism as the lipoyl domains of both E2 and E3BP can indeed reach all type of active sites in PDHc, their efficiency in doing so varies.

Substrate-Driven Coupling

Although PDHc has been studied in great detail as a prototype for substrate channeling in multi-enzyme assemblies, it is not fully understood how lipoyl arms sample “productive conformations” in the course of the reaction. As they have to reach distant active sites at E1, E2, and E3 for completion of the multi-step reaction, a pure stochastic movement would result in many non-productive interactions between lipoyl moiety and active sites. A visit of, e.g., E2 active site by non-acetylated lipoyl domain, or of E3 active site by acetylated lipoyl domain, will be catalytically unproductive.

We observed that binding of substrate CoA to the core changes significantly the amount of crosslinks between lipoyl domains of E2 and E3BP with E1, E2, and E3 lipoyl entrance sites (Figure 6B and Table S2). As it is known that the lipoyl entrance gate at E2 opens in the presence of CoA from the studies on related branched chain α -ketoacid dehydrogenase complex (Kato et al., 2006), the crosslinks between the lipoyl domains of E2 and the lipoyl entrance site of the IC domain expectedly increased by as much as ~2.5-fold. Surprisingly, the crosslinks between E3 and lipoyl domains of E2 and E3BP also increased by a factor of ~2 and ~41, respectively. Most likely, the enhanced affinity of E2 lipoyl domains toward the open gate of CoA-bound E2 increases their residence time, providing more freedom for the E3BP lipoyl domain to visit E3. This scenario is also supported by the observed ~0.4-fold decrease in inter-lipoyl-domain interactions in the presence of CoA. In the multi-step catalytic cycle of PDHc, the binding and acetylation of CoA occurs after oxidative decarboxylation of pyruvate at E1. Thus, it would seem logical that CoA binding to E2 aids in subsequent substeps by promoting lipoyl domains of E2 and E3BP to visit the E2 and E3 active sites with higher frequency.

Hence, a substrate-binding event, in this case CoA, affects the conformational and chemical landscapes of the lipoyl domain meshwork such that the subsequent steps of multi-step PDHc reaction become favored. The conformation sampling of lipoyl domains is therefore not entirely stochastic, but is also affected by and synchronized with substrate binding and catalysis. It remains to be studied inasmuch binding of E1 and E3 substrates also reorganizes the conformational landscape of the PDHc multi-enzyme assembly, and whether this interplay between substrate binding/catalysis and conformational sampling is a general principle of multi-enzyme machines with highly flexible substrate shuttles, such as lipoyl or acyl carrier protein domains.

Conclusion

Here, we find by a combination of biophysical analysis, structural biology, and native and crosslinking mass spectrometry that the structural architecture of the human PDHc core does not contain a uniform distribution of E2 and E3BP constituents. This imbalanced distribution of E2 and E3BP translates into sets of local E1 and E3 clusters at the periphery of the PDHc. In addition, we find that the structural dynamics of the PDHc is not entirely stochastic as implied by the proposed MRC mechanism, but is modulated by the presence of substrates, in particular CoA. Consequently, the structural asymmetry and substrate-induced modulation of the conformational landscape primes the PDHc for the individual partial reactions with enhanced efficiency and streamlines substrate channeling between the different components.

STAR★METHODS

Detailed methods are provided in the online version of this paper and include the following:

- KEY RESOURCES TABLE
- CONTACTS FOR REAGENT AND RESOURCE SHARING
- METHOD DETAILS
 - Protein Overexpression
 - Protein Purifications
 - In-Vitro Reconstitution of Human PDH Complex and Sub-Complexes
 - Isothermal Titration Calorimetry
 - Negative Staining Electron Microscopy (Neg-Staining EM)
 - Cryo-Electron Microscopy (Cryo-EM)
 - 3-D Model Building
 - Crosslinking Mass Spectrometry (XL-MS)
 - Native Mass Spectrometry (Native MS)
- QUANTIFICATION AND STATISTICAL ANALYSIS
- DATA AND SOFTWARE AVAILABILITY

SUPPLEMENTAL INFORMATION

Supplemental Information can be found online at <https://doi.org/10.1016/j.str.2019.04.009>.

ACKNOWLEDGMENTS

This study was funded by the Deutsche Forschungsgemeinschaft (SFB 860 to K.T. and H.S.), the Federal Ministry of Education and Research (03Z22HN22 to

C.S.) and the European Funds for Regional Developments (ZS/2016/04/78115 to C.S.). D.H. was partially supported by a scholarship from Boehringer Ingelheim Fonds. We would also like to thank Dr. Uwe Jandt (TUHH) for sharing atomic coordinates of human E2 and E3BP from their MD simulation study.

AUTHOR CONTRIBUTIONS

K.T. designed and coordinated the project together with H.S. and C.S. S.P. recombinantly expressed all proteins and characterized them biochemically and biophysically. S.P. prepared samples for EM and mass spectrometry. D.H. and H.S. carried out EM experiments and calculated the derived structural models. S.P., D.H., A.C., H.S., and K.T. analyzed the structural data. S.W. and C.S. conducted all mass spectrometry experiments and analyzed the data. All authors contributed to the interpretation of the functional, structural, and mass spectrometry data. S.P. and K.T. wrote the paper with input from all co-authors. All authors reviewed and edited the manuscript and approved its final form.

DECLARATION OF INTERESTS

The authors declare no competing interests.

Received: July 8, 2018

Revised: January 17, 2019

Accepted: April 11, 2019

Published: May 23, 2019

REFERENCES

- Afonine, P.V., Grosse-Kunstleve, R.W., Adams, P.D., and Urzhumtsev, A. (2013). Bulk-solvent and overall scaling revisited: faster calculations, improved results. *Acta Crystallogr. D Biol. Crystallogr.* **69**, 625–634.
- Allen, A.G., Perham, R.N., Allison, N., Miles, J.S., and Guest, J.R. (1989). Reductive acetylation of tandemly repeated lipoyl domains in the pyruvate-dehydrogenase multienzyme complex of *Escherichia coli* is random order. *J. Mol. Biol.* **208**, 623–633.
- Bates, D.L., Danson, M.J., Hale, G., Hooper, E.A., and Perham, R.N. (1977). Self-assembly and catalytic activity of pyruvate-dehydrogenase multienzyme complex of *Escherichia coli*. *Nature* **268**, 313–316.
- Brautigam, C.A., Wynn, R.M., Chuang, J.L., and Chuang, D.T. (2009). Subunit and catalytic component stoichiometries of an in vitro reconstituted human pyruvate dehydrogenase complex. *J. Biol. Chem.* **284**, 13086–13098.
- Ciszak, E.M., Makal, A., Hong, Y.S., Vettaikkorumakankavu, A.K., Korotchkina, L.G., and Patel, M.S. (2006). How dihydrolipoamide dehydrogenase-binding protein binds dihydrolipoamide dehydrogenase in the human pyruvate dehydrogenase complex. *J. Biol. Chem.* **281**, 648–655.
- Collins, J.H., and Reed, L.J. (1977). Acyl group and electron pair relay system – network of interacting lipoyl moieties in pyruvate and alpha-ketoglutarate dehydrogenase complexes from *Escherichia coli*. *Proc. Natl. Acad. Sci. U S A* **74**, 4223–4227.
- Danson, M.J., Fersht, A.R., and Perham, R.N. (1978). Rapid intra-molecular coupling of active-sites in pyruvate-dehydrogenase complex of *Escherichia coli*—mechanism for rate enhancement in multimeric structure. *Proc. Natl. Acad. Sci. U S A* **75**, 5386–5390.
- Demarco, O., and Lindsay, J.G. (1985). Component-X—an immunologically distinct polypeptide associated with mammalian pyruvate-dehydrogenase multi-enzyme complex. *Eur. J. Biochem.* **149**, 641–648.
- Emsley, P., and Cowtan, K. (2004). Coot: model-building tools for molecular graphics. *Acta Crystallogr. D Biol. Crystallogr.* **60**, 2126–2132.
- Frank, R.A.W., Pratap, J.V., Pei, X.Y., Perham, R.N., and Luisi, B.F. (2005). The molecular origins of specificity in the assembly of a multienzyme complex. *Structure* **13**, 1119–1130.
- Guest, J.R., Lewis, H.M., Graham, L.D., Packman, L.C., and Perham, R.N. (1985). Genetic reconstruction and functional-analysis of the repeating lipoyl domains in the pyruvate-dehydrogenase multienzyme complex of *Escherichia coli*. *J. Mol. Biol.* **185**, 743–754.

- Hackert, M.L., Oliver, R.M., and Reed, L.J. (1983a). A computer-model analysis of the active-site coupling mechanism in the pyruvate-dehydrogenase multienzyme complex of *Escherichia coli*. *Proc. Natl. Acad. Sci. U S A* 80, 2907–2911.
- Hackert, M.L., Oliver, R.M., and Reed, L.J. (1983b). Evidence for a multiple random coupling mechanism in the alpha-ketoglutarate dehydrogenase multienzyme complex of *Escherichia coli*—a computer-model analysis. *Proc. Natl. Acad. Sci. U S A* 80, 2226–2230.
- Harris, R.A., Bowker-Kinley, M.M., Wu, P., Jeng, J., and Popov, K.M. (1997). Dihydrolipoamide dehydrogenase-binding protein of the human pyruvate dehydrogenase complex. DNA-derived amino acid sequence, expression, and reconstitution of the pyruvate dehydrogenase complex. *J. Biol. Chem.* 272, 19746–19751.
- Hernandez, H., and Robinson, C.V. (2007). Determining the stoichiometry and interactions of macromolecular assemblies from mass spectrometry. *Nat. Protoc.* 2, 715–726.
- Hezaveh, S., Zeng, A.P., and Jandt, U. (2016). Human pyruvate dehydrogenase complex E2 and E3BP core subunits: new models and insights from molecular dynamics simulations. *J. Phys. Chem. B* 120, 4399–4409.
- Hiromasa, Y., Fujisawa, T., Aso, Y., and Roche, T.E. (2004). Organization of the cores of the mammalian pyruvate dehydrogenase complex formed by E2 and E2 plus the E3-binding protein and their capacities to bind the E1 and E3 components. *J. Biol. Chem.* 279, 6921–6933.
- Jilka, J.M., Rahmatullah, M., Kazemi, M., and Roche, T.E. (1986). Properties of a newly characterized protein of the bovine kidney pyruvate-dehydrogenase complex. *J. Biol. Chem.* 261, 1858–1867.
- Kastner, B., Fischer, N., Golas, M.M., Sander, B., Dube, P., Boehringer, D., Hartmuth, K., Deckert, J., Hauer, F., Wolf, E., et al. (2008). GraFix: sample preparation for single-particle electron cryomicroscopy. *Nat. Methods* 5, 53–55.
- Kato, M., Wynn, R.M., Chuang, J.L., Brautigam, C.A., Custorio, M., and Chuang, D.T. (2006). A synchronized substrate-gating mechanism revealed by cubic-core structure of the bovine branched-chain alpha-ketoacid dehydrogenase complex. *EMBO J.* 25, 5983–5994.
- Kato, M., Wynn, R.M., Chuang, J.L., Tso, S.C., Machius, M., Li, J., and Chuang, D.T. (2008). Structural basis for inactivation of the human pyruvate dehydrogenase complex by phosphorylation: role of disordered phosphorylation loops. *Structure* 16, 1849–1859.
- Kim, D.E., Chivian, D., and Baker, D. (2004). Protein structure prediction and analysis using the Robetta server. *Nucleic Acids Res.* 32, W526–W531.
- Kong, Y., Ming, D., Wu, Y., Stoops, J.K., Zhou, Z.H., and Ma, J. (2003). Conformational flexibility of pyruvate dehydrogenase complexes: a computational analysis by quantized elastic deformational model. *J. Mol. Biol.* 330, 129–135.
- Korkes, S., Del Campillo, A., Gunsalas, I.C., and Ochoa, S. (1951). Enzymatic synthesis of citric acid. IV. Pyruvate as acetyl donor. *J. Biol. Chem.* 193, 721–735.
- Korotchkina, L.G., Tucker, M.M., Thekkumkara, T.J., Madhusudhan, K.T., Pons, G., Kim, H., and Patel, M.S. (1995). Overexpression and characterization of human tetrameric pyruvate dehydrogenase and its individual subunits. *Protein Exp. Purif.* 6, 79–90.
- Liu, S., Baker, J.C., and Roche, T.E. (1995). Binding of the pyruvate dehydrogenase kinase to recombinant constructs containing the inner lipoyl domain of the dihydrolipoyl acetyltransferase component. *J. Biol. Chem.* 270, 793–800.
- Mande, S.S., Sarfaty, S., Allen, M.D., Perham, R.N., and Hol, W.G. (1996). Protein-protein interactions in the pyruvate dehydrogenase multienzyme complex: dihydrolipoamide dehydrogenase complexed with the binding domain of dihydrolipoamide acetyltransferase. *Structure* 4, 277–286.
- Mattevi, A., Obmolova, G., Schulze, E., Kalk, K.H., Westphal, A.H., de Kok, A., and Hol, W.G. (1992). Atomic structure of the cubic core of the pyruvate dehydrogenase multienzyme complex. *Science* 255, 1544–1550.
- Miles, J.S., Guest, J.R., Radford, S.E., and Perham, R.N. (1988). Investigation of the mechanism of active-site coupling in the pyruvate-dehydrogenase multienzyme complex of *Escherichia coli* by protein engineering. *J. Mol. Biol.* 202, 97–106.
- Morgner, N., and Robinson, C.V. (2012). Massign: an assignment strategy for maximizing information from the mass spectra of heterogeneous protein assemblies. *Anal. Chem.* 84, 2939–2948.
- Nawa, H., Brady, W.T., Koike, M., and Reed, L.J. (1960). Studies on the nature of protein-bound lipoic acid. *J. Am. Chem. Soc.* 82, 896–903.
- Neagle, J., Demarco, O., Dunbar, B., and Lindsay, J.G. (1989). Component-X of mammalian pyruvate-dehydrogenase complex—structural and functional-relationship to the lipoate acetyltransferase (E2) component. *FEBS Lett.* 253, 11–15.
- Neagle, J.C., and Lindsay, J.G. (1991). Selective proteolysis of the protein X subunit of the bovine heart pyruvate dehydrogenase complex. Effects on dihydrolipoamide dehydrogenase (E3) affinity and enzymic properties of the complex. *Biochem. J.* 278 (Pt 2), 423–427.
- Olsen, J.V., de Godoy, L.M., Li, G., Macek, B., Mortensen, P., Pesch, R., Makarov, A., Lange, O., Horning, S., and Mann, M. (2005). Parts per million mass accuracy on an Orbitrap mass spectrometer via lock mass injection into a C-trap. *Mol. Cell. Proteomics* 4, 2010–2021.
- Patel, M.S., and Korotchkina, L.G. (2006). Regulation of the pyruvate dehydrogenase complex. *Biochem. Soc. Trans.* 34, 217–222.
- Petersen, E.F., Goddard, T.D., Huang, C.C., Couch, G.S., Greenblatt, D.M., Meng, E.C., and Ferrin, T.E. (2004). UCSF Chimera—a visualization system for exploratory research and analysis. *J. Comput. Chem.* 25, 1605–1612.
- Rahmatullah, M., Gopalakrishnan, S., Andrews, P.C., Chang, C.L., Radke, G.A., and Roche, T.E. (1989). Subunit associations in the mammalian pyruvate-dehydrogenase complex—structure and role of protein-X and the pyruvate-dehydrogenase component binding domain of the dihydrolipoyl transacetylase component. *J. Biol. Chem.* 264, 2221–2227.
- Rahmatullah, M., Radke, G.A., Andrews, P.C., and Roche, T.E. (1990). Changes in the core of the mammalian-pyruvate dehydrogenase complex upon selective removal of the lipoyl domain from the transacetylase component but not from the protein X component. *J. Biol. Chem.* 265, 14512–14517.
- Reed, L.J. (1966). Macromolecular organization of enzyme systems. *Annu. Rev. Biochem.* 35, 57–84.
- Reed, L.J. (1974). Multienzyme complexes. *Acc. Chem. Res.* 7, 40–46.
- Reed, L.J., and Hackert, M.L. (1990). Structure-function-relationships in dihydrolipoamide acyltransferases. *J. Biol. Chem.* 265, 8971–8974.
- Reid, E.E., Lytle, C.R., Canvin, D.T., and Dennis, D.T. (1975). Pyruvate-dehydrogenase complex activity in proplasts and mitochondria of developing castor bean endosperm. *Biochem. Biophys. Res. Commun.* 62, 42–47.
- Scheres, S.H. (2012). RELION: implementation of a Bayesian approach to cryo-EM structure determination. *J. Struct. Biol.* 180, 519–530.
- Seifert, F., Ciszak, E., Korotchkina, L., Golbik, R., Spinka, M., Dominiak, P., Sidhu, S., Brauer, J., Patel, M.S., and Tittmann, K. (2007). Phosphorylation of serine 264 impedes active site accessibility in the E1 component of the human pyruvate dehydrogenase multienzyme complex. *Biochemistry* 46, 6277–6287.
- Seifert, F., Golbik, R., Brauer, J., Lilie, H., Schroder-Tittmann, K., Hinze, E., Korotchkina, L.G., Patel, M.S., and Tittmann, K. (2006). Direct kinetic evidence for half-of-the-sites reactivity in the E1 component of the human pyruvate dehydrogenase multienzyme complex through alternating sites cofactor activation. *Biochemistry* 45, 12775–12785.
- Smolle, M., Prior, A.E., Brown, A.E., Cooper, A., Byron, O., and Lindsay, J.G. (2006). A new level of architectural complexity in the human pyruvate dehydrogenase complex. *J. Biol. Chem.* 281, 19772–19780.
- Sobott, F., Hernandez, H., McCammon, M.G., Tito, M.A., and Robinson, C.V. (2002). A tandem mass spectrometer for improved transmission and analysis of large macromolecular assemblies. *Anal. Chem.* 74, 1402–1407.
- Song, J., and Jordan, F. (2012). Interchain acetyl transfer in the E2 component of bacterial pyruvate dehydrogenase suggests a model with different roles for each chain in a trimer of the homooligomeric component. *Biochemistry* 51, 2795–2803.

- Stepp, L.R., Bleile, D.M., McRorie, D.K., Pettit, F.H., and Reed, L.J. (1981). Use of trypsin and lipoamidase to study the role of lipoic acid moieties in the pyruvate and alpha-ketoglutarate dehydrogenase complexes of *Escherichia coli*. *Biochemistry* 20, 4555–4560.
- Stoops, J.K., Cheng, R.H., Yazdi, M.A., Maeng, C.Y., Schroeter, J.P., Klueppelberg, U., Kolodziej, S.J., Baker, T.S., and Reed, L.J. (1997). On the unique structural organization of the *Saccharomyces cerevisiae* pyruvate dehydrogenase complex. *J. Biol. Chem.* 272, 5757–5764.
- Studier, F.W. (2005). Protein production by auto-induction in high density shaking cultures. *Protein Exp. Purif.* 41, 207–234.
- Texter, F.L., Radford, S.E., Laue, E.D., Perham, R.N., Miles, J.S., and Guest, J.R. (1988). Site-directed mutagenesis and H-1-NMR spectroscopy of an interdomain segment in the pyruvate-dehydrogenase multienzyme complex of *Escherichia coli*. *Biochemistry* 27, 289–296.
- Vijayakrishnan, S., Callow, P., Nutley, M.A., McGow, D.P., Gilbert, D., Kropholler, P., Cooper, A., Byron, O., and Lindsay, J.G. (2011). Variation in the organization and subunit composition of the mammalian pyruvate dehydrogenase complex E2/E3BP core assembly. *Biochem. J.* 437, 565–574.
- Vijayakrishnan, S., Kelly, S.M., Gilbert, R.J., Callow, P., Bhella, D., Forsyth, T., Lindsay, J.G., and Byron, O. (2010). Solution structure and characterisation of the human pyruvate dehydrogenase complex core assembly. *J. Biol. Chem.* 399, 71–93.
- Wagenknecht, T., Grassucci, R., Radke, G.A., and Roche, T.E. (1991). Cryoelectron microscopy of mammalian pyruvate-dehydrogenase complex. *J. Biol. Chem.* 266, 24650–24656.
- Wang, J.J., Nemeria, N.S., Chandrasekhar, K., Kumaran, S., Arjunan, P., Reynolds, S., Calero, G., Brukh, R., Kakalis, L., Furey, W., et al. (2014). Structure and function of the catalytic domain of the dihydrolipoyl acetyltransferase component in *Escherichia coli* pyruvate dehydrogenase complex. *J. Biol. Chem.* 289, 15215–15230.
- Yang, B., Wu, Y.J., Zhu, M., Fan, S.B., Lin, J.Z., Zhang, K., Li, S., Chi, H., Li, Y.X., Chen, H.F., et al. (2012). Identification of cross-linked peptides from complex samples. *Nat. Methods* 9, 904–906.
- Yu, X.K., Hiromasa, Y., Tsen, H., Stoops, J.K., Roche, T.E., and Zhou, Z.H. (2008). Structures of the human pyruvate dehydrogenase complex cores: a highly conserved catalytic center with flexible N-terminal domains. *Structure* 16, 104–114.
- Zhang, K. (2016). Gctf: real-time CTF determination and correction. *J. Struct. Biol.* 193, 1–12.
- Zhou, Z.H., Liao, W., Cheng, R.H., Lawson, J.E., McCarthy, D.B., Reed, L.J., and Stoops, J.K. (2001a). Direct evidence for the size and conformational variability of the pyruvate dehydrogenase complex revealed by three-dimensional electron microscopy. The “breathing” core and its functional relationship to protein dynamics. *J. Biol. Chem.* 276, 21704–21713.
- Zhou, Z.H., McCarthy, D.B., O'Connor, C.M., Reed, L.J., and Stoops, J.K. (2001b). The remarkable structural and functional organization of the eukaryotic pyruvate dehydrogenase complexes. *Proc. Natl. Acad. Sci. U S A* 98, 14802–14807.

STAR★METHODS**KEY RESOURCES TABLE**

REAGENT or RESOURCE	SOURCE	IDENTIFIER
Chemicals, Peptides, and Recombinant Proteins		
Coenzyme A trilithium salt dihydrate	PanReac AppliChem	CAS 18439-24-2
Aluminum oxide	Sigma-Aldrich	CAS 11028
Polyethylene glycol 6000	Carl Roth	CAS 25322-68-3
Glutaraldehyde	Sigma-Aldrich	CAS 111-30-8
Bis(sulfosuccinimidyl)suberate	Thermo Fisher Scientific	CAS 82436-77-9
Trypsin	Promega	CAS 9002-07-7
RapiGest surfactant	Waters corp.	CAS 308818-13-5
Ammonium acetate, 7.5 M	Sigma-Aldrich	CAS 631-61-8
Acetonitrile	Sigma-Aldrich	CAS 75-05-8
Water, HPLC grade	Merck	CAS 7732-18-5
TFA, HPLC grade	Sigma-Aldrich	CAS 76-05-1
Formic acid, Optima LCMS grade	Fisher scientific	CAS 64-18-6
Bacterial and Virus Strains		
E. coli: BL21 Star (DE3)	ThermoFisher	Cat. C6010-03
M15	D. Stüber, F. Hoffmann-La Roche Ltd	N/A
Deposited Data		
Structure of E2 ₆₀ core	this study	PDB: 6H55
Structure of E3BP ₆₀ core	this study	PDB: 6H60
Crystal structure of PDHc E2 from <i>Azotobacter vinelandii</i>	Mattevi et al., 1992,	PDB: 1EAD
Crystal structure of PDHc E2 from <i>Escherichia coli</i>	Wang et al., 2014	PDB: 4N72
Pseudo-atomic structure of human PDHc E2	Yu et al., 2008	PDB: 3B8K
Cryo-EM map of human PDHc E2 ₆₀ -E3BP ₂₀ core	this study	EMD: 0138
Recombinant DNA		
pQE-9-6HE1alphaE1beta	Korotchkina et al., 1995	N/A
pPDHE2-E3BP	Harris et al., 1997	N/A
pET28a_hE3	GeneArt	N/A
Software and Algorithms		
MicroCal Analysis	Malvern	N/A
PyMOL	The PyMOL Molecular Graphics System, Version 2.0, Schrödinger, LLC	https://pymol.org/ RRID: SCR_000305
UCSF Chimera	Pettersen et al., 2004	https://www.cgl.ucsf.edu/chimera/ RRID: SCR_004097
Robetta server	Kim et al., 2004	robbetta.bakerlab.org
GCtf	Zhang, 2016	https://www.mrc-lmb.cam.ac.uk/kzhang/
Cow beta	Luettich et al. (Unpublished)	www.cow-em.de
Gautomatch	Dr Kai Zhang	https://www.mrc-lmb.cam.ac.uk/kzhang/
Relion v2.02	Scheres 2012	http://www2.mrc-lmb.cam.ac.uk/relion/index.php/Main_Page
Coot v0.8.8	Emsley and Cowtan, 2004	https://www2.mrc-lmb.cam.ac.uk/personal/emsley/coot/
pLink 1	Yang et al., 2012	http://pfind.ict.ac.cn/software/pLink/
MassLynxx v4.0	Waters	N/A
Massign	Morgner and Robinson, 2012	http://massign.chem.ox.ac.uk/
XCalibur v4.0.27.13	Thermo Fisher Scientific	N/A

(Continued on next page)

Continued

REAGENT or RESOURCE	SOURCE	IDENTIFIER
Other		
Mortar Grinder RM 200	Retsch GmbH	N/A
Gradient Master 108	BioComp	N/A
iTC200 microcalorimeter	Malvern	N/A
Phillips CM200 FEG EM	Phillips/FEI	N/A
Titan Krios	FEI/Thermo Scientific	N/A
EM-GP	Leica	N/A
Orbitrap Fusion Tribrid Mass Spectrometer	Thermo scientific	N/A
G1 mass spectrometer	Waters	N/A
Ultima mass spectrometer	Waters	N/A
Dionex UltiMate 3000 RSLC	Thermo Scientific	N/A
Micro Bio-spin 6 columns	Bio-Rad	Cat. No. 7326228
Superdex peptide column 10/300 GL	GE Healthcare	Cat. No. 17517601
Reprosil C18, particle size 5 μm	Dr. Maisch	N/A
Reprosil C18, particle size 1.9 μm	Dr. Maisch	N/A

CONTACTS FOR REAGENT AND RESOURCE SHARING

Further information and requests for specific resources and reagents should be directed to and will be fulfilled by the lead contact, Kai Tittmann (ktittma@gwdg.de).

METHOD DETAILS**Protein Overexpression**

The mixed E2-E3BP core and E3 were overexpressed in *E. coli* strain BL21DE3* (Invitrogen) using an auto-induction protocol modified from (Studier, 2005). In brief, cells were grown overnight in LB medium at 37°C in the presence of required antibiotics (35 $\mu\text{g}/\mu\text{L}$ chloramphenicol for E2-E3BP or 50 $\mu\text{g}/\mu\text{L}$ kanamycin for E3). The overnight culture was used to inoculate an auto-induction medium consisting of TB medium, 1xNPS solution [0.025 M (NH₄)₂SO₄], 0.05 M Na₂HPO₄ and 0.05 M KH₂PO₄], 1x5052 [0.5 % (w/v) glycerol, 0.05 % (w/v) glucose and 0.2 % (w/v) lactose], antibiotics (vide supra) and 1 mM MgSO₄. Lipoic acid (0.6 mM) was added for expression of E2-E3BP. The cells were grown at 37°C until the culture reached an OD₆₀₀ of 0.6-0.8. Thereafter, the temperature was lowered to 18°C and the cells were grown for another 65-70 hours. The cells were then harvested by centrifugation at 4800 RPM and 4°C in JLA 8.1000 rotor (Beckman-Coulter). E1 was overexpressed under high cell density conditions using fed-batch fermentation as described before (Seifert et al., 2006). Plasmids for co-expressing E2 and E3BP (pPDHE2-E3BP) and hE1 (pQE-9-6HE1alphaE1beta) were kindly provided by Prof. Dr. Mulchand Patel ([Harris et al., 1997](https://www.ncbi.nlm.nih.gov/pmc/articles/PMC1997232/); [Korotchkina et al., 1995](https://www.ncbi.nlm.nih.gov/pmc/articles/PMC1995232/)). pET28a-hE3 plasmid encoding human E3 was synthesized by GeneArt and produces a protein with an N-terminal poly-histidine tag.

Protein Purifications

E1 purification was carried out as reported before (Seifert et al., 2006). Cells (5-10 g) producing E3 were suspended in lysis buffer (50 mM Na₂PO₄, pH 8.0, 20 mM imidazole, 200 mM NaCl) supplemented with 1 mM PMSF. The cell suspension was incubated with a spatula tip lysozyme and DNase I, and stirred on ice for at least 30 min. The cells were lysed by passing through a fluidizer (Microfluidics Corp., USA) at 70-80 psi for three cycles, and cell debris was removed by centrifugation at 45000 g at 6°C for 30 min. The clear supernatant was loaded onto the His-trap column (GE Healthcare) pre-washed with lysis buffer followed by a linear gradient of 0-100 % elution buffer (50 mM Na₂PO₄, pH 8.0, 200 mM NaCl, 100 mM imidazole) over 10 column volumes. The elution peaks were analyzed by SDS-PAGE and the pure fractions were pooled. The volume was reduced to < 1 mL by ultrafiltration using Spin-X® UF concentrator with MWCO of 50 kDa, and loaded onto a S-200 gel filtration column pre-equilibrated with 3 column volumes of final buffer (50 mM Na₂PO₄, pH 8, 200 mM NaCl). The elution peaks were evaluated using SDS-PAGE, and pure fractions were concentrated to 20-30 mg/mL, and stored on ice until eventual usage.

E2-E3BP overexpressing cells (~ 40 g) were mixed with 100 g alumina and 20 ml of lysis buffer (50 mM HEPES, pH 7.5, 150 mM KCl, 20 mM Mg(OAc)₂, 30 mM NH₄Cl, 1 mM DTE and 1 mM PMSF), and grinded manually in a mortar using a pestle to reach a dough-like consistency. Then, the mortar and pestle were mounted to a Mortar Grinder RM 200 (Retsch GmbH), and the cells were grinded for 45 min. After 35 min, lysozyme and DNase I (spatula tip each) were added along with 80 mL of lysis buffer. The cell suspension was transferred to 50 mL Falcon tubes and centrifuged at 9000 RPM (1620 A rotor, Hettich GmbH &Co. KG), 6°C for 30 min to

remove alumina and cell debris. The supernatant was again centrifuged at 45000g, 6°C for 30 min to remove the remaining cell debris. The supernatant was adjusted to room temperature, and 0.1 % (w/v) protamine sulfate was added and stirred at room temperature for 30 min. Afterwards, the solution was centrifuged at 15.000g, 20°C for 20 min. The clear supernatant was incubated on ice for 10 min, and icecold PEG-6000 (50 % stock) was added in a step-wise manner to initially adjust 4 %, and in the final step 6 %. At each fractionation step, the protein suspension was stirred for 30 min in a cold room followed by centrifugation at 15.000 x g, 4°C for 20 min. Final buffer (50 mM HEPES, pH 7.5, 150 mM KCl and 1 mM DTE) was added to the pellet obtained by precipitation with 6 % PEG-6000, and re-suspended by gentle shaking. When the protein had been completely solubilized, it was layered on the top of a 10-30 % linear sucrose gradient in a SW-40 rotor tube, and centrifuged at 20.000 rpm, 4°C for 16 hr. The sucrose solutions were prepared in the final buffer, and the linear gradient was made by 'Gradient Master 108' according to the manufacturer's manual (BioComp, Canada). Once the ultracentrifugation had been finished, the gradient was fractionated from the top with 400 µL fraction size using a micropipette. These fractions were subjected to SDS-PAGE analysis, and the pure fractions were pooled. PEG-6000 (50 % stock) was added to the pooled protein to adjust a concetration of 8 %. The sample was then centrifuged at 15.000g, 4°C for 20 min, and the protein pellet was solubilized in the final buffer. Further centrifugation at 15.000 rpm (1420 B, Hettich GmbH & Co. KG), 4°C for 15 min was performed to remove insoluble material. The supernatant containing soluble protein was transferred to fresh Eppendorf tubes and kept on ice until further usage.

In-Vitro Reconstitution of Human PDH Complex and Sub-Complexes

E1 and E3 proteins were incubated in 3-5 times molar excess relative to their binding sites at E2-E3BP core (assuming the E2₄₀-E3BP₂₀ model). The protein mixture was placed on top of a linear 10-30% sucrose gradient in SW-40 rotor tubes, and centrifuged at 20.000 rpm and 4°C for 16 hr. The fractionation and PEG precipitation of pure fractions were carried out as described for the E2-E3BP core. The sucrose solutions and the protein resuspensions were prepared in high-salt buffer (50 mM HEPES, pH 7.5, 300 mM KCl and 1 mM DTE). This buffer was supplemented with 0.1 mM ThDP, 1 mM MgCl₂, 2 mM CoA and 0.2 mM NAD⁺. The same procedure was followed for reconstituting E1-core sub-complex except that no NAD⁺ was added. When reconstituting the E2-E3BP core with E3, low salt buffer 50 mM HEPES, pH 7.5, 150 mM KCl and 1 mM DTE was used with a buffer as described above but devoid of ThDP and MgCl₂. The purity of the protein complexes after reconstitution were confirmed by denaturing polyacryl amide gel electrophoresis (Figure S6).

Isothermal Titration Calorimetry

All PDHc proteins were dialyzed using a membrane chamber (ZelluTrans/Roth® dialysis membrane, MWCO 3.5 kDa), in 50 mM HEPES, 150 mM KCl, pH 7.5 buffer. The CoA solution was freshly prepared in the post-dialysis buffer. The sample cell of the iTC200 microcalorimeter (Malvern) was filled with ~ 0.5-2 µM human PDHc core solution. 1.5 µL of either 2 mM CoA or 140-210 µM E3 were injected in a series of 24 injections with constant stirring at 500 RPM. Temperature was maintained at 25°C for analysis of protein-protein interactions and 30°C for analysis of CoA binding. Control experiments comprised an identical setup but with the sample cell being filled with post-dialysis buffer instead of protein. Subtraction of heat of dilution, base line correction and curve fitting were all performed using the MicroCal Analysis software.

Negative Staining Electron Microscopy (Neg-Staining EM)

40-100 pmoles protein complex were chemically crosslinked by ultracentrifugation on 10-30 % linear sucrose with a 0-0.02% glutar-aldehyde gradient in a method described as GraFix (Kastner et al., 2008). The fractions were analyzed using dot blot via amido black staining. The protein particles from a chosen fraction were then bound to a thin carbon film for 30-60 sec. The protein-soaked film was transferred to an electron microscopic grid covered with a Holey support carbon film. The protein-containing surface of the grid was stained with saturated uranyl formate solution (in water) for 1-2 min, excess liquid removed and then air dried. Images were recorded at a magnification of 88,000-fold on a 4k x 4k CCD camera (TVIPS GmbH) using two-fold pixel binning (2,45 Å/pixel) in a Phillips CM200 FEG electron microscope (Philips/FEI) operated at 160 kV acceleration voltage.

Cryo-Electron Microscopy (Cryo-EM)

The E2-E3BP mixed core sample was buffer-exchanged to remove sucrose from the GraFix step, and then vitrified on continuous carbon foil on a quantifoil grid (3.5/1) in a FEI Vitrobot mark IV at a blot force of 13 and a blot time of 8.5 s. Roughly 2250 micrographs were recorded on a Titan Krios microscope equipped with a Cs corrector and a Falcon I detector at 300kV, 59.000x (pixel size: 1.27 Å/px) with a dose of 41 e/Å². Subsequently, 212.468 particles were selected using the software John Henry (custom written in the Stark lab), and an initial model was constructed using angular reconstitution method in software suite cow eyes (custom written in Stark lab). False positives were removed from this initial model by 2D classification. Remaining good particles were subjected to 3D classification in Relion (Scheres, 2012), imposing icosahedral symmetry and the best class was refined. The final map consisted of 29.788 particles with a resolution of 6.3 Å.

3-D Model Building

Initial homology modelling was performed using Robetta (robbetta.bakerlab.org). C-terminal 233 amino acid residues of E2 and E3BP were used as input in the server for structure predictions. The software identified PDB: 3B8K as a template and generated homology models of E2 and E3BP core forming domains as output. These monomers were assembled in UCSF Chimera and molecular

dynamics flexible fitting (MDFF) was used to fit the model into the map. Real-space refinement was performed for thus obtained final model using Phenix (Afonine et al., 2013). Visualization of EM density map was done in UCSF Chimera (Pettersen et al., 2004) and the structural models were aligned and compared using PyMol (Schrödinger).

Crosslinking Mass Spectrometry (XL-MS)

Human PDHc was incubated on ice for approx. 5 min in the presence or absence of 2 mM CoA. Proteins were then cross-linked with 5 mM bis-(sulfosuccinimidyl)suberate (BS3) for 1h at 25°C and 300 rpm in a thermomixer. Proteins were then precipitated with ethanol and digested with trypsin (1:20 stoichiometry trypsin:protein) using RapiGest surfactant (Waters corp.) according to the manufacturer's protocols. Peptides were dissolved in 30 % ACN/0.1 % TFA, and cross-linked di-peptides were enriched by size exclusion chromatography at a flow rate of 50 μ l/min using a Superdex 10/300 GL peptide column (GE healthcare). Fractions containing cross-linked peptides were dried in a vacuum centrifuge and re-dissolved in 2 % (v/v) ACN / 0.05 % TFA. Peptides were separated by nano-flow reversed-phase liquid chromatography (Dionex UltiMate 3000 RSLC, Thermo scientific). The mobile phases included mobile phase A: 0.1 % (v/v) formic acid and mobile phase B: 80 % (v/v) acetonitrile and 0.08 % (v/v) formic acid. Afterwards, the peptides were loaded onto a trap column (Reprosil C18, 100 μ m I.D., particle size 5 μ m; Dr. Maisch GmbH, prepared in-house) and separated on an analytical C18 capillary column (Reprosil C18, 75 μ m I.D., particle size 1.9 μ m, 27-28 cm; Dr. Maisch GmbH, prepared in-house), with a gradient of 5-90 % (v/v) mobile phase B over 75 min at flow rate of 300 nL/min. Setup included direct elution of thus separated peptides into an Orbitrap Fusion Tribrid Mass Spectrometer (Thermo scientific).

Mass spectrometry was operated in data-dependent mode with spray voltage of 2.0 kV, capillary temperature at 275°C and normalized collision energy as 30 % at an activation of $q = 0.25$ and an activation time of 30 ms. Survey full-scan MS spectra were acquired in the orbitrap (m/z 350–1550) with a resolution of 120,000 and an automatic gain control (AGC) target at 500,000. The top 20 most intense ions were selected for HCD MS/MS fragmentation in the orbitrap at an AGC target of 30,000 and with a first m/z of 110. Previously selected ions within previous 30 s were dynamically excluded for 20 s. Only the ions with charge states of 3–8 were selected. Internal calibration was performed for orbitrap using the lock mass option (lock mass: m/z 445.120025) (Olsen et al., 2005).

Raw data files were converted into ‘mgf’ file format using pXtract software tool (<http://pfind.ict.ac.cn/software.html>). By searching against a reduced database containing Atg18, potential cross-links were recognized with pLink search engine (Yang et al., 2012). Search parameters were as follows: fragmentation: HCD, enzyme: trypsin, variable modifications: oxidation (methionine) and carbamidomethylation (cysteine) and cross-linker: BS3. Finally, confirmation of spectra of possible crosslinked di-peptides was done manually. Only those crosslinks, which have at least one good spectrum with a pLink score of <1e-3, were considered in the final output.

For quantification of selected crosslinks, extracted ion chromatograms of m/z values corresponding to crosslinks identified in +/- CoA states were generated using Xcalibur v4.0.27.13 (Thermo Fisher Scientific) using standard parameters. Extracted ion chromatograms were generated for multiple charge states of the identified cross-links, if available. Intensity ratios for identified cross-links (+CoA versus -CoA or vice versa) from peak areas of extracted ion chromatograms.

Native Mass Spectrometry (Native MS)

The purification buffer of human PDHc and subcomplexes was exchanged against 200 mM ammonium acetate (pH 7) using Micro Bio-spin 6 columns (Bio Rad). Spectra were acquired on a G1 or an Ultima mass spectrometer (Waters) modified for transmission of high masses (Sobott et al., 2002) using in-house prepared gold-coated glass capillaries (Hernandez and Robinson, 2007). Typical mass spectrometric parameters for G1 were capillary voltage, 1.7 kV; cone voltage, 150 V; extractor, 40 V; trap collision energy, 20 V; transfer collision energy, 15 V; source backing pressure, 7–10 mbar; trap gas, 0.5 mL/min. Typical mass spectrometric parameters for Ultima were capillary voltage, 1.5–1.7 kV; cone voltage, 80 V; RF lens 1, 80 V; collision energy, 50–180 V; aperture 3, 13.6 V. Acquired mass spectra were processed and complexes were assigned using MassLynx (Waters) and Masssign software (Morgner and Robinson, 2012).

QUANTIFICATION AND STATISTICAL ANALYSIS

All ITC experiments were conducted with minimum three replications to calculate stoichiometry between CoA and its binding sites in E2-E3BP core and E2 core. The associated standard error of mean is also provided alongside the calculated stoichiometry.

Statistics of electron microscopy data collection, model building, refinement and validation are provided in Table S4.

Statistical details are provided, wherever required, in the STAR Methods.

DATA AND SOFTWARE AVAILABILITY

The cryo-EM density map of E2₄₀-E3BP₂₀ core generated in this study has been deposited in the Electron Microscopy Data Bank under ID code EMD: 0138.

The pseudo-atomic structures of human PDHc E2 and E3BP subunits generated in this study have been deposited in the Protein Data bank under ID codes PDB: 6H55 and PDB: 6H60, respectively.